Strong constraints from COSINE-100 on the DAMA dark matter results using the same sodium iodide target

Govinda Adhikari
Department of Physics, Sejong University
E. Barbosa de Souza
Yale University
N. Carlin
University of Sao Paulo
J.J. Choi
Seoul National University
S. Choi
Seoul National University
M. Djamal
Bandung Institute of Technology
Anthony C. Ezeribe
University of Sheffield https://orcid.org/0000-0003-1604-2304
L.E. Franca
University of Sao Paulo
C. Ha
Chung-Ang University
I.S. Hahn
Ewha Womans University
E.J. Jeon
Institute for Basic Science
J.H. Jo
Yale University
H.W. Joo
Seoul National University
W.G. Kang
Institute for Basic Science
M. Kauer
University of Wisconsin–Madison
H. Kim

Institute for Basic Science

H.J. Kim
Kyungpook National University

K.W. Kim
Institute for Basic Science https://orcid.org/0000-0001-7639-9511

S.H. Kim
Institute for Basic Science

S.K. Kim
Seoul National University

W.K. Kim
University of Science and Technology

Y.D. Kim
Institute for Basic Science

Y.H. Kim
Institute for Basic Science

Young Ju Ko
Institute for Basic Science https://orcid.org/0000-0002-5055-8745

E.K. Lee
Institute for Basic Science

H. Lee
University of Science and Technology

Hyun Su Lee (hyunsulee@ibs.re.kr)
Institute for Basic Science https://orcid.org/0000-0002-0444-8473

H.Y. Lee
Institute for Basic Science

I.S. Lee
Institute for Basic Science

J Lee
Institute for Basic Science

J.Y. Lee
Kyungpook National University

M.H. Lee
Institute for Basic Science

S.H. Lee
University of Science and Technology

S.M. Lee
Seoul National University

D Leonard
Institute for Basic Science

B. Manzato
University of Sao Paulo
R. Maruyama
Yale University
R. Neal
University of Sheffield
S. Olsen
Institute for Basic Science
B.J. Park
University of Science and Technology
H.K. Park
Korea University
H.S. Park
Korea Research Institute of Standards and Science
K.S. Park
Institute for Basic Science
R. Pitta
University of Sao Paulo
H. Prihtiadi
Bandung Institute of Technology
SeJin Ra
Institute for Basic Science https://orcid.org/0000-0002-3490-7968
C. Rott
Sungkyunkwan University
K.A. Shin
Institute for Basic Science
A. Scarff
University of Sheffield
N. Spooner
University of Sheffield
William Thompson
Yale University https://orcid.org/0000-0003-2988-7998
L. Yang
University of California San Diego
G.H. Yu
Sungkyunkwan University

Article

Keywords: COSINE-100, DAMA, dark matter physics

Posted Date: April 23rd, 2021

DOI: https://doi.org/10.21203/rs.3.rs-429107/v1

Version of Record: A version of this preprint was published at Science Advances on November 12th, 2021. See the published version at https://doi.org/10.1126/sciadv.abk2699.

Strong constraints from COSINE-100 on the DAMA dark matter results using the same sodium iodide target

G. Adhikari,[1] E. Barbosa de Souza,[2] N. Carlin,[3] J. J. Choi,[4] S. Choi,[4] M. Djamal,[5] A. C. Ezeribe,[6] L. E. França,[3] C. Ha,[7] I. S. Hahn,[8,9,10] E. J. Jeon,[11] J. H. Jo,[2] H. W. Joo,[4] W. G. Kang,[11] M. Kauer,[12] H. Kim,[11] H. J. Kim,[13] K. W. Kim,[11] S. H. Kim,[11] S. K. Kim,[4] W. K. Kim,[10,11] Y. D. Kim,[11,14,10] Y. H. Kim,[11,15,10] Y. J. Ko,[11,a)] E. K. Lee,[11] H. Lee,[10,11] H. S. Lee,[11,10,b)] H. Y. Lee,[11] I. S. Lee,[11] J. Lee,[11] J. Y. Lee,[13] M. H. Lee,[11,10] S. H. Lee,[10,11] S. M. Lee,[4] D. S. Leonard,[11] B. B. Manzato,[3] R. H. Maruyama,[2] R. J. Neal,[6] S. L. Olsen,[11] B. J. Park,[10,11] H. K. Park,[16] H. S. Park,[15] K. S. Park,[11] R. L. C. Pitta,[3] H. Prihtiadi,[11] S. J. Ra,[11] C. Rott,[17] K. A. Shin,[11] A. Scarff,[6] N. J. C. Spooner,[6] W. G. Thompson,[2] L. Yang,[1] and G. H. Yu[17]

(COSINE-100 Collaboration)

[1)] *Department of Physics, University of California San Diego, La Jolla, CA 92093, USA*

[2)] *Department of Physics and Wright Laboratory, Yale University, New Haven, CT 06520, USA*

[3)] *Physics Institute, University of São Paulo, 05508-090, São Paulo, Brazil*

[4)] *Department of Physics and Astronomy, Seoul National University, Seoul 08826, Republic of Korea*

[5)] *Department of Physics, Bandung Institute of Technology, Bandung 40132, Indonesia*

[6)] *Department of Physics and Astronomy, University of Sheffield, Sheffield S3 7RH, United Kingdom*

[7)] *Department of Physics, Chung-Ang University, Seoul 06973, Republic of Korea*

[8)] *Department of Science Education, Ewha Womans University, Seoul 03760, Republic of Korea*

[9)] *Center for Exotic Nuclear Studies, Institute for Basic Science (IBS), Daejeon 34126, Republic of Korea*

[10)] *IBS School, University of Science and Technology (UST), Daejeon 34113,*

Republic of Korea

[11] *Center for Underground Physics, Institute for Basic Science (IBS), Daejeon 34126, Republic of Korea*

[12] *Department of Physics and Wisconsin IceCube Particle Astrophysics Center, University of Wisconsin-Madison, Madison, WI 53706, USA*

[13] *Department of Physics, Kyungpook National University, Daegu 41566, Republic of Korea*

[14] *Department of Physics, Sejong University, Seoul 05006, Republic of Korea*

[15] *Korea Research Institute of Standards and Science, Daejeon 34113, Republic of Korea*

[16] *Department of Accelerator Science, Korea University, Sejong 30019, Republic of Korea*

[17] *Department of Physics, Sungkyunkwan University, Suwon 16419, Republic of Korea*

[a] Electronic mail: yjko@ibs.re.kr

[b] Electronic mail: hyunsulee@ibs.re.kr

It is a long-standing debate as to whether or not the annual modulation in the event rate observed by the DAMA sodium iodide experiment[1,2] is caused by the interaction of dark matter particles. To resolve this issue, several groups have been working to develop new experiments with the aim of reproducing or refuting DAMA's results using the same sodium iodide target medium[3–7]. The COSINE-100 experiment is one of these that is currently operating with 106 kg of low-background sodium iodide crystals at the Yangyang underground laboratory[8,9]. Analysis of the initial 59.5 days of COSINE-100 data showed that the annual modulation signal reported by DAMA is inconsistent with explanation using spin-independent interaction of weakly interacting massive particles (WIMPs), a favored candidate of dark matter particles[10,11], with sodium or iodine nuclei in the context of the standard halo model[8]. However, this first result left open interpretations using certain alternative dark matter models[12], dark matter halo distributions[13], and detector responses[13,14] that could allow room for consistency between DAMA and COSINE-100. Here we present new results from over 1.7 years of COSINE-100 operation with improved event selection and energy threshold reduced from 2 keV to 1 keV[15]. We find an order of magnitude improvement in sensitivity, sufficient for the first time to strongly constrain these alternative scenarios, as well as to further strengthen the previously observed inconsistency with the WIMP-nucleon spin-independent interaction hypothesis[8].

COSINE-100 is located at the Yangyang Underground Laboratory in South Korea with about 700 m rock overburden[8,9]. The experiment consists of eight low-background thallium-doped sodium iodide (NaI(Tl)) crystals arranged in a 4×2 array with a total target mass of 106 kg. The array is immersed in 2,200 L of liquid scintillator used to identify events induced by radioactive backgrounds inside or outside the crystals[16]. The liquid scintillator is surrounded by copper, lead, and plastic scintillators to reduce the background contribution from external radiation as well as cosmic-ray muons[17]. Each NaI(Tl) crystal is optically coupled to two photomultiplier tubes (PMTs) with the signals recorded as 8 μs waveforms. A trigger is generated when a signal corresponding to one or more photoelectrons occurs in each PMT within a 200 ns time window[18].

The analysis presented here utilizes the 1.7 years of data previously used for the first annual modulation search[9] and the background modeling with 1 keV energy threshold[19].

This data was acquired from October 21, 2016 to July 18, 2018. Three of the eight crystals were observed to have high noise rates in the region of interest (ROI) and so were excluded from the analysis, resulting in an effective data exposure of 97.7 kg·year[8,9].

In the ROI, it was found that PMT noise causes the majority of triggers. A multivariable boosted decision tree (BDT)[20] was used to characterize the pulse-shapes to discriminate these PMT-induced noise events from radiation-induced scintillation events[8,9]. To improve discrimination power, new parameters are introduced as input training variables to the BDT. It is a likelihood score that the waveform matches either scintillation events or PMT-induced noise events. The likelihood score particularly enhances separation of the noise and allows us to achieve a 1 keV threshold[15]. The BDT is trained with samples of scintillation-rich ^{60}Co calibration data and PMT-noise dominant single-hit physics data. The multiple-hit events consist of hits in multiple crystals or liquid scintillator that are not caused by the dark matter interactions. Event selection efficiency for the scintillation events is evaluated with the ^{60}Co calibration dataset and cross-checked with the physics data, as well as nuclear recoil events. The efficiencies from the ^{60}Co calibration data were found to be consistent with previously measured efficiencies for nuclear recoil events obtained using a monoenergetic 2.42 MeV neutron beam[21] (see Extended Data Fig. 2). The efficiency differences and their uncertainties are included as a systematic uncertainty (See Methods).

Events in the remaining dark matter search dataset predominantly originate from environmental γ and β radiations. Sources include radioactive contaminants internal to the crystals or on their surfaces, external detector components, and cosmogenic activation[19]. In order to understand this, the background spectrum for each individual crystal is modeled using computer simulations based on the Geant4 toolkit[22]. Multiple-hit events with measured energies between 1 and 3,000 keV and single-hit events between 6 and 3,000 keV are used in the modeling. Single-hit events with energies below 6 keV are excluded in the modeling to avoid a bias against dark matter signal events. Details of the procedure used for the background modeling are provided elsewhere[19] (see also Extended Data Fig. 3).

Several sources of systematic uncertainties are identified and included in this analysis. The largest systematic uncertainties are those associated with the efficiency, which include statistical errors in the efficiency determination with the ^{60}Co calibration and systematic errors derived from the independent cross-checks of the physics data and the nuclear recoil events. Uncertainties in the energy resolution and nonlinear responses of the NaI(Tl) crys-

tals[23] affect the shapes of the background and signal spectra. The depth-profiles of ^{210}Pb on the surface of the NaI(Tl) crystals, studied with a ^{222}Rn contaminated crystal, are varied within their uncertainty[24]. Variations in the levels and the positions of external Uranium and Thorium decay-chain contaminants are also accounted. Effects of event rate variations and possible distortions in the shapes of spectra are considered in systematic uncertainties (see Methods).

We consider various WIMP models to determine the possible contribution of the WIMP interactions to the measured energy spectra using the simulated data (see Methods). The DAMA/LIBRA-phase2 data[2] were found not to be compatible with the canonical model[14,25], which is an isospin-conserving spin-indpendent interaction between WIMP and nucleus in the specific context of the standard WIMP galactic halo model, and is the most widely used in the interpretation of the direct detection of the WIMP dark matter[26]. However, an isospin-violating interaction noting that the WIMP-proton coupling is different from the WIMP-neutron coupling, allows a good fit to the observed annual modulation signals from the DAMA/LIBRA-phase2 data[14,25]. To interpret the DAMA/LIBRA data and compare with the COSINE-100 data, we use the best fit values of the effective coupling of WIMPs to neutrons and to protons (f_n/f_p) obtained for the simultaneous fit of DAMA/LIBRA-phase1 and DAMA/LIBRA-phase2 data described elsewhere[14]. We also interpret the results of the COSINE-100 data in the canonical model for the comparison with the DAMA/LIBRA-phase1 only data.

We use the nuclear recoil quenching factor (QF) from recent measurements with monoenergetic neutron beams[21] (quenching factor is the ratio of the scintillation light yield from sodium or iodine recoil relative to that for electron recoil for the same energy). In those measurements, neutron tagging detectors at a fixed angle relative to the incoming neutron beam direction provide unambiguous knowledge of deposited energy. Modelings of the QF measurements described in Ref.[14] are appropriated for this analysis (subsequently referred to as new QF). However, most studies interpreting the DAMA/LIBRA's results have used significantly large QF values reported by the DAMA group in 1996[27] (subsequently referred to as DAMA QF), that were obtained by measuring the response of NaI(Tl) crystals to nuclear recoils induced by neutrons from a ^{252}Cf source. For example, the sodium and iodine QF values were reported by DAMA to be 30% and 9%, but by the new measurements to be approximately 13% and 5%, respectively, at 20 keV nuclear recoil energy[14]. The measure-

ments of the DAMA QF values were required to check the trigger and selection efficiencies in low-energy regions and consider energy dependent QF as pointed in Ref.[28]. However, a hypothesis of different QFs[13] in the NaI(Tl) crystals used by DAMA/LIBRA and COSINE-100 needs to be checked. Note that results from analysis of the previous 59.5 days of COSINE-100 data with a 2 keV threshold were not sufficient to exclude all the DAMA/LIBRA 3σ regions when different QFs are used[14].

To search for evidence of WIMP signal from the data, a Bayesian approach with a likelihood function based on Poisson probability is used. The likelihood fit is performed to the measured single-hit energy spectra between 1 and 15 keV for each WIMP model for several masses. Each crystal is fitted with crystal-specific background model and crystal-correlated WIMP signal for the combined fit by multiplying the five crystals' likelihoods. Means and uncertainties for background components, which are determined from the modeling[19], are used to set Gaussian priors for the background. The systematic uncertainties are included in the fit as nuisance parameters with Gaussian prior (see Methods).

A good fit to the DAMA/LIBRA-phase2 data was obtained with the isospin-violating interaction[14,25]. We simultaneously use the DAMA/LIBRA-phase1 and phase2 data to fit three parameters: the WIMP mass, the WIMP-proton cross-section, and f_n/f_p. The best fits were obtained for two different values of f_n/f_p favoring WIMP-sodium and WIMP-iodine interactions as $f_n/f_p = -0.76$ and -0.71, respectively. For the best fit values of f_n/f_p, the 3σ allowed regions in the WIMP-mass and the WIMP-proton cross-section parameter spaces are obtained[14].

The COSINE-100 data are fitted to each of the different WIMP masses for each f_n/f_p value using only the new QF values. An example of a maximum likelihood fit with a 11.5 GeV/c^2 and $f_n/f_p = -0.76$ WIMP signal is presented in Fig. 1. The summed event spectrum for the five crystals is shown together with the best-fit result. For comparison, the expected signal for a 11.5 GeV/c^2 WIMP with a spin-independent WIMP-proton cross section of 2.5×10^{-2} pb, the central value of the DAMA/LIBRA best fit using the DAMA QF values for the WIMP-sodium interaction, is shown by the red solid line. No excess of events that could be attributed to WIMP interactions are found for the considered WIMP signals. The posterior probabilities of signals are consistent with zero in all cases and 90% confidence level limits are determined (see Extended Data Fig. 5). Figure 2 shows the 3σ contours of the DAMA/LIBRA data in the best fit values of f_n/f_p using the new QF values and the

DAMA QF values together with the 90% confidence level upper limits from the COSINE-100 data using the same f_n/f_p and the new QF values. The 90% confidence level limits from the 1.7 years COSINE-100 data show approximately an order of magnitude better limits than those of our previous results using 59.5 days data and exclude the DAMA/LIBRA allowed 3σ regions for both of the two different QF values.

Even though the DAMA/LIBRA-phase2 data do not fit with the canonical model, the DAMA/LIBRA-phase1 data has been shown to be well fit with an isospin-conserving spin-independent WIMP-nuclei interaction[14,29]. The 90% confidence level upper limits from the COSINE-100 data for the canonical model are also obtained. Figure 3 shows the 3σ allowed regions that are associated with the DAMA/LIBRA-phase1 signal using the new QF values and the DAMA QF values together with the 90% confidence level upper limits from the COSINE-100 data using the new QF values. These limits mostly exclude the DAMA/LIBRA allowed region even though different QF values are considered for each experiment.

In addition, we have checked each operator in non-relativistic effective field theory models where previous null results from the 59.5 days COSINE-100 data do not fully cover the $3\,\sigma$ regions of the DAMA/LIBRA data for a few operators[12]. The 1.7 years data is now found to fully cover the $3\,\sigma$ allowed regions assuming same DAMA QF values as one can see in Fig. 4.

After releasing the initial 59.5 days COSINE-100 data with null observations using the same NaI(Tl) target material, a few possibilities have been raised to allow consistency between the DAMA/LIBRA and COSINE-100 results[12–14]. The results of this analysis, with 1.7 years accumulated COSINE-100 data and improved analysis technique with 1 keV energy threshold, do not favor the suggested possibilities. A model independent data analysis of the annual modulation with several years COSINE-100 data is required for an unambiguous conclusion, nevertheless these results provide strong constraints on the dark matter interpretation of the DAMA/LIBRA annual modulation signals with the same NaI(Tl) target materials.

REFERENCES

[1]R. Bernabei et al., (DAMA/LIBRA Collaboration), Final model independent result of DAMA/LIBRA-phase1, Eur. Phys. J. C **73**, 2648 (2013).

[2]R. Bernabei et al., (DAMA/LIBRA Collaboration), First Model Independent Results from DAMA/LIBRA-Phase2, Nucl. Phys. At. Energy **19**, 307 (2018).

[3]K. W. Kim et al., Tests on NaI(Tl) crystals for WIMP search at the Yangyang Underground Laboratory, Astropart. Phys. **62**, 249 (2015).

[4]G. Adhikari et al., (COSINE-100 Collaboration), Initial Performance of the COSINE-100 Experiment, Eur. Phys. J. C **78**, 107 (2018).

[5]B. Suerfu, M. Wada, W. Peloso, M. Souza, F. Calaprice, J. Tower, and G. Ciampi, Growth of Ultra-high Purity NaI(Tl) Crystal for Dark Matter Searches, Phys. Rev. Research **2**, 013223 (2020).

[6]K. Fushimi et al., Development of highly radiopure NaI(Tl) scintillator for PICOLON dark matter search project, `arXiv:2101.00759`.

[7]J. Amare et al., Annual Modulation Results from Three Years Exposure of ANAIS-112, `arXiv:2103.01175`.

[8]G. Adhikari et al., (COSINE-100 Collaboration), An experiment to search for dark-matter interactions using sodium iodide detectors, Nature **564**, 83 (2018).

[9]G. Adhikari et al., (COSINE-100 Collaboration), Search for a dark matter-induced annual modulation signal in NaI(Tl) with the COSINE-100 experiment, Phys. Rev. Lett. **123**, 031302 (2019).

[10]B. W. Lee and S. Weinberg, Cosmological lower bound on heavy-neutrino masses, Phys. Rev. Lett. **39**, 165 (1977).

[11]M. W. Goodman and E. Witten, Detectability of Certain Dark Matter Candidates, Phys. Rev. D **31**, 3059 (1985).

[12]G. Adhikari et al., (COSINE-100 and Sogang Phenomenology Group Collaboration), COSINE-100 and DAMA/LIBRA-phase2 in WIMP effective models, JCAP **1906**, 048 (2019).

[13]R. Bernabei et al., The DAMA project: Achievements, implications and perspectives, Prog. Part. Nucl. Phys. **114**, 103810 (2020).

[14]Y. J. Ko et al., (COSINE-100 Collaboration), Comparison between DAMA/LIBRA and COSINE-100 in the light of Quenching Factors, JCAP **1911**, 008 (2019).

[15]G. Adhikari et al., (COSINE-100 Collaboration), Lowering the energy threshold in COSINE-100 dark matter searches, Astropart. Phys. **130**, 102581 (2021).

[16]G. Adhikari et al., (COSINE-100 Collaboration), The COSINE-100 Liquid Scintillator

Veto System, arXiv:2004.03463.

[17]H. Prihtiadi et al., (COSINE-100 Collaboration), Muon detector for the COSINE-100 experiment, JINST **13**, T02007 (2018).

[18]G. Adhikari et al., (COSINE-100 Collaboration), The COSINE-100 Data Acquisition System, JINST **13**, P09006 (2018).

[19]G. Adhikari et al., (COSINE-100 Collaboration), Background modeling for dark matter search with 1.7 years of cosine-100 data, arXiv:2101.11377.

[20]J. H. Friedman, Greedy function approximation: A gradient boosting machine, Ann. Stat. **29**, 1189 (2001).

[21]H. W. Joo, H. S. Park, J. H. Kim, S. K. Kim, Y. D. Kim, H. S. Lee, and S. H. Kim, Quenching factor measurement for NaI(Tl) scintillation crystal, Astropart. Phys. **108**, (2019).

[22]S. Agostinelli et al., (GEANT4 Collaboration), GEANT4: A Simulation toolkit, Nucl. Instrum. Meth. A **506**, 250 (2003).

[23]L. Swiderski, Response of doped alkali iodides measured with gamma-ray absorption and Compton electrons, Nucl. Instrum. Meth. A **705**, 42 (2013).

[24]G. H. Yu, C. Ha, E. J. Jeon, K. W. Kim, N. Y. Kim, Y. D. Kim, H. S. Lee, H. K. Park, and C. Rott, Depth profile study of ^{210}Pb in the surface of an NaI(Tl) crystal, Astropart. Phys. **126**, 102518 (2021).

[25]S. Baum, K. Freese, and C. Kelso, Dark Matter implications of DAMA/LIBRA-phase2 results, Phys. Lett. B **789**, 262–269 (2019).

[26]M. Tanabashi et al., (Particle Data Group Collaboration), Review of Particle Physics, Phys. Rev. D **98**, 030001 (2018).

[27]R. Bernabei et al., (DAMA Collaboration), New limits on WIMP search with large-mass low-radioactivity NaI(Tl) set-up at Gran Sasso, Phys. Lett. B **389**, 757 – 766 (1996).

[28]J. I. Collar, Quenching and channeling of nuclear recoils in NaI(Tl): Implications for dark-matter searches, Phys. Rev. C **88**, 035806 (2013).

[29]C. Savage, G. Gelmini, P. Gondolo, and K. Freese, Compatibility of DAMA/LIBRA dark matter detection with other searches, JCAP **0904**, 010 (2009).

[30]E. Barbosa de Souza et al., (COSINE-100 Collaboration), Study of cosmogenic radionuclides in the COSINE-100 NaI(Tl) detectors, Astropart. Phys. **115**, 102390 (2020).

ACKNOWLEDGMENTS

We thank the Korea Hydro and Nuclear Power (KHNP) Company for providing underground laboratory space at Yangyang. This work is supported by: the Institute for Basic Science (IBS) under project code IBS-R016-A1 and NRF-2016R1A2B3008343, Republic of Korea; NSF Grants No. PHY-1913742, DGE-1122492, WIPAC, the Wisconsin Alumni Research Foundation, United States; STFC Grant ST/N000277/1 and ST/K001337/1, United Kingdom; Grant No. 2017/02952-0 FAPESP, CAPES Finance Code 001, CNPq 131152/2020-3, Brazil.

AUTHOR INFORMATION

Contributions The COSINE-100 detector was designed and constructed by the COSINE-100 collaboration. Operation, data processing, calibration and detector simulation were performed by the COSINE-100 collaboration members. The main analysis was lead by G.A and Y.J.K with strong guidance and review by the collaboration members. The paper was written by Y.J.K and H.S.L and edited by other members of the collaboration. All authors have participated in online shift and approved the manuscript. Authors are alphabetically listed by their last names.

Competing interests The authors declare no competing interests.

Correspondence and requests for materials should be addressed to Y.J.K and H.S.L.

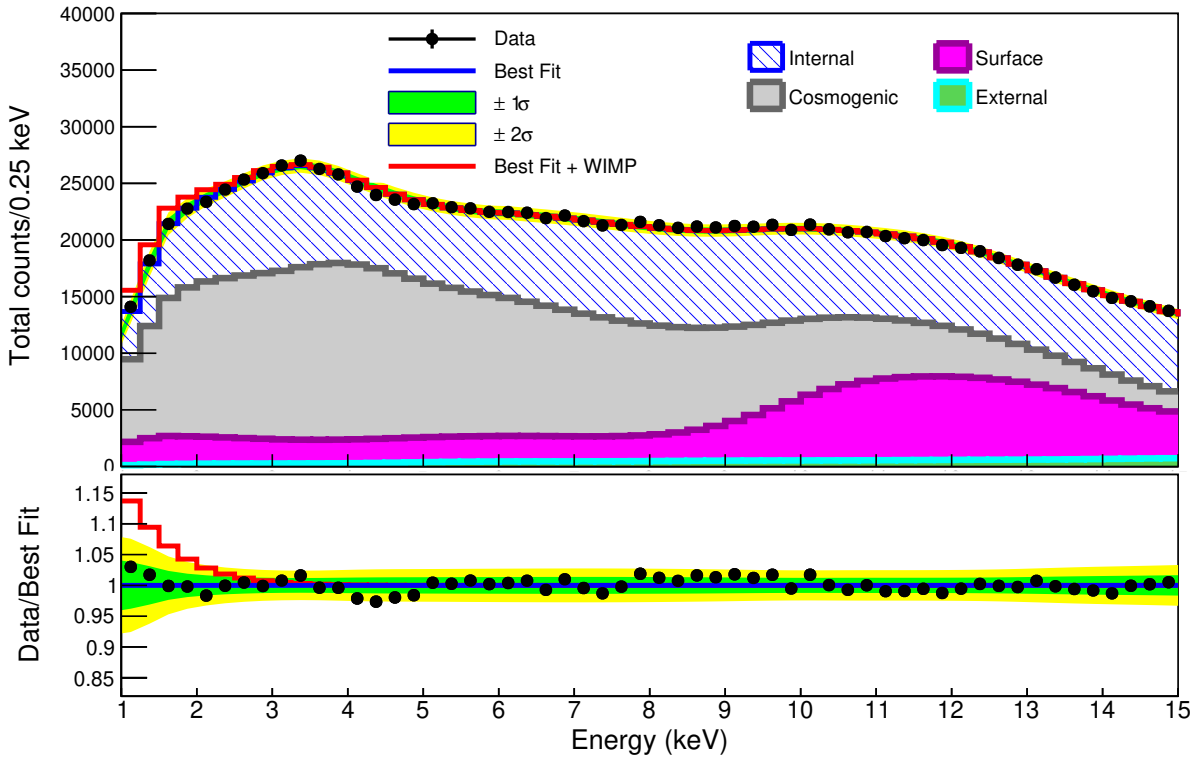

FIG. 1. **Example fit results for a 11.5 GeV/c^2 WIMP mass in the case of $f_n/f_p = -0.76$.** Presented here are the summed energy spectrum for the five crystals (black filled circles shown with 68% confidence level error bars) and the best fit (blue line) for which no WIMP signals are obtained. Fitted contributions to the background from internal radionuclide contaminations, the surface of the crystals and nearby materials, cosmogenic activation, and external backgrounds are indicated. The green (yellow) bands are the 68% (95%) confidence level intervals of the systematic uncertainty obtained from the likelihood fit. As a presentation purpose, we indicate the signal shape (red line) assuming a WIMP-proton cross section of 2.5×10^{-2} pb corresponding to the DAMA best fit value for the WIMP-sodium interaction using the DAMA QF values.

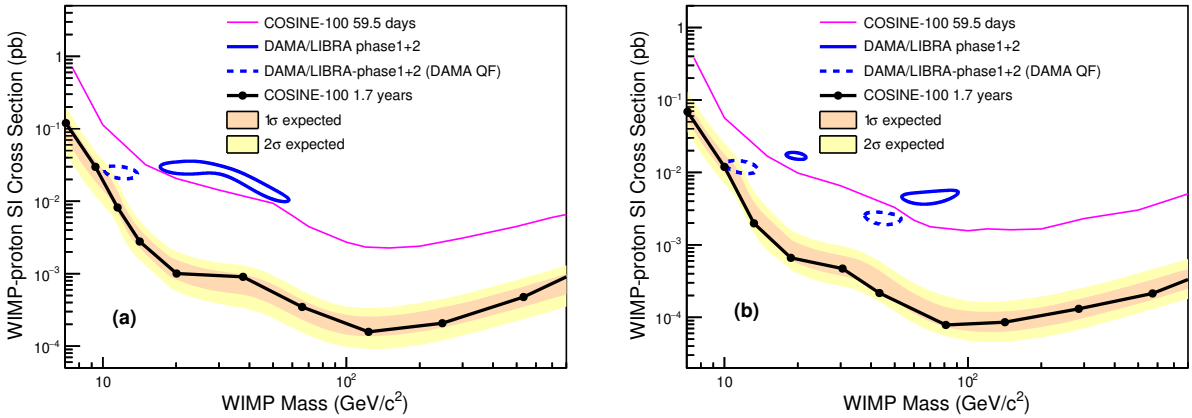

FIG. 2. **Exclusion limits on the WIMP-proton spin-independent cross section for the isospin-violating interaction.** The 3σ allowed regions of the WIMP mass and the WIMP-proton cross-section associated with the DAMA/LIBRA-phase1+phase2 data (blue solid coutours) using the new QF values in their best fit for (a) sodium scattering and (b) iodine scattering hypotheses are compared with the 90% confidence level exclusion limits from the COSINE-100 data (black-solid-line), together with the 68% and 95% probability bands for the expected 90% confidence level limit assuming the background-only hypothesis. The dashed blue contours show the allowed regions of the DAMA/LIBRA-phase1+phase2 data using the DAMA QF values. For comparison, limits from the initial 59.5 days COSINE-100 data[8] are shown by the purple-solid-line. In each plot, we fix the effective coupling ratios to neutrons and protons f_n/f_p to the best fit values of the DAMA data.

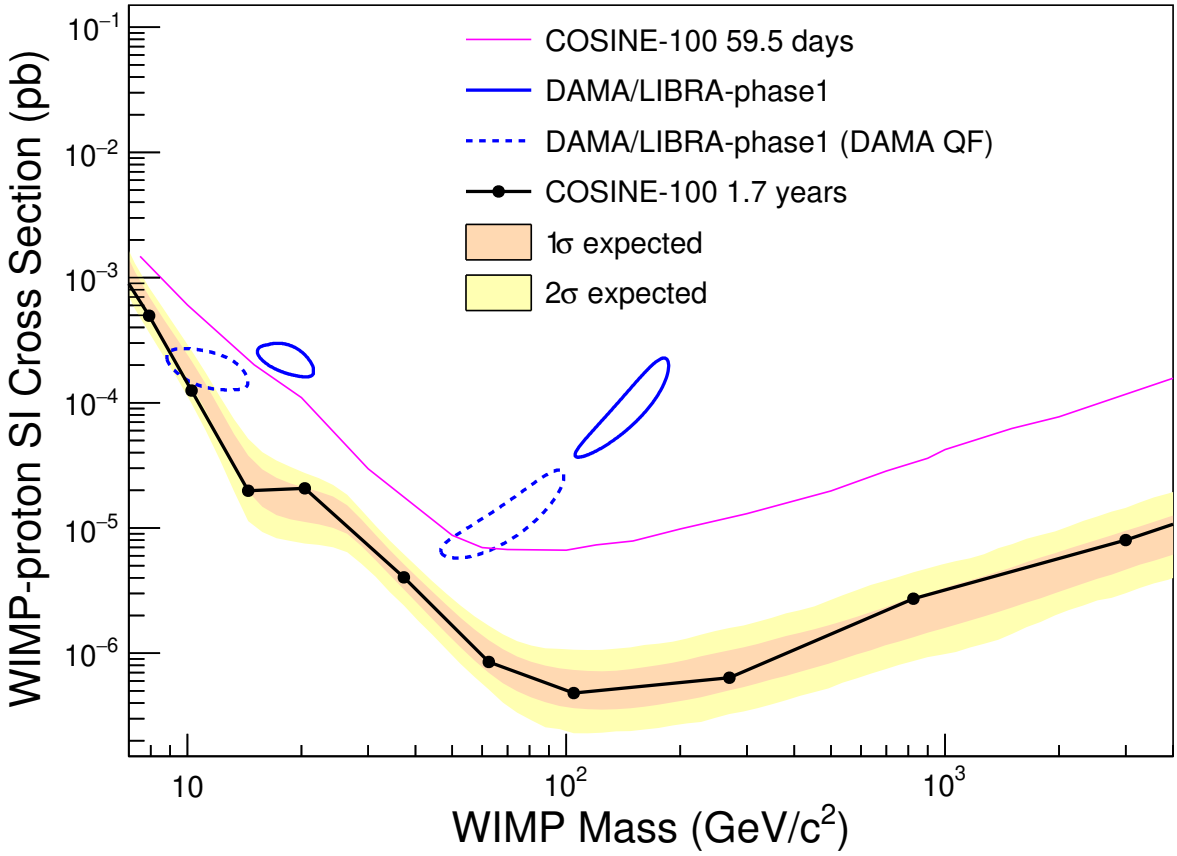

FIG. 3. **Exclusion limits on the WIMP-nucleon spin-independent cross section of the isospin-conserving interaction.** The observed (filled circles with black solid line) 90% confidence level exclusion limits on the WIMP-nucleon spin-independent cross section from the COSINE-100 are shown together with the 68% and 95% probability bands for the expected 90% confidence level limit, assuming the background-only hypothesis. The limits are compared with a WIMP interpretation of the DAMA/LIBRA-phase1 3σ allowed region using the new QF (blue-solid-contours) and the DAMA QF (blue-dashed-contours)[29].

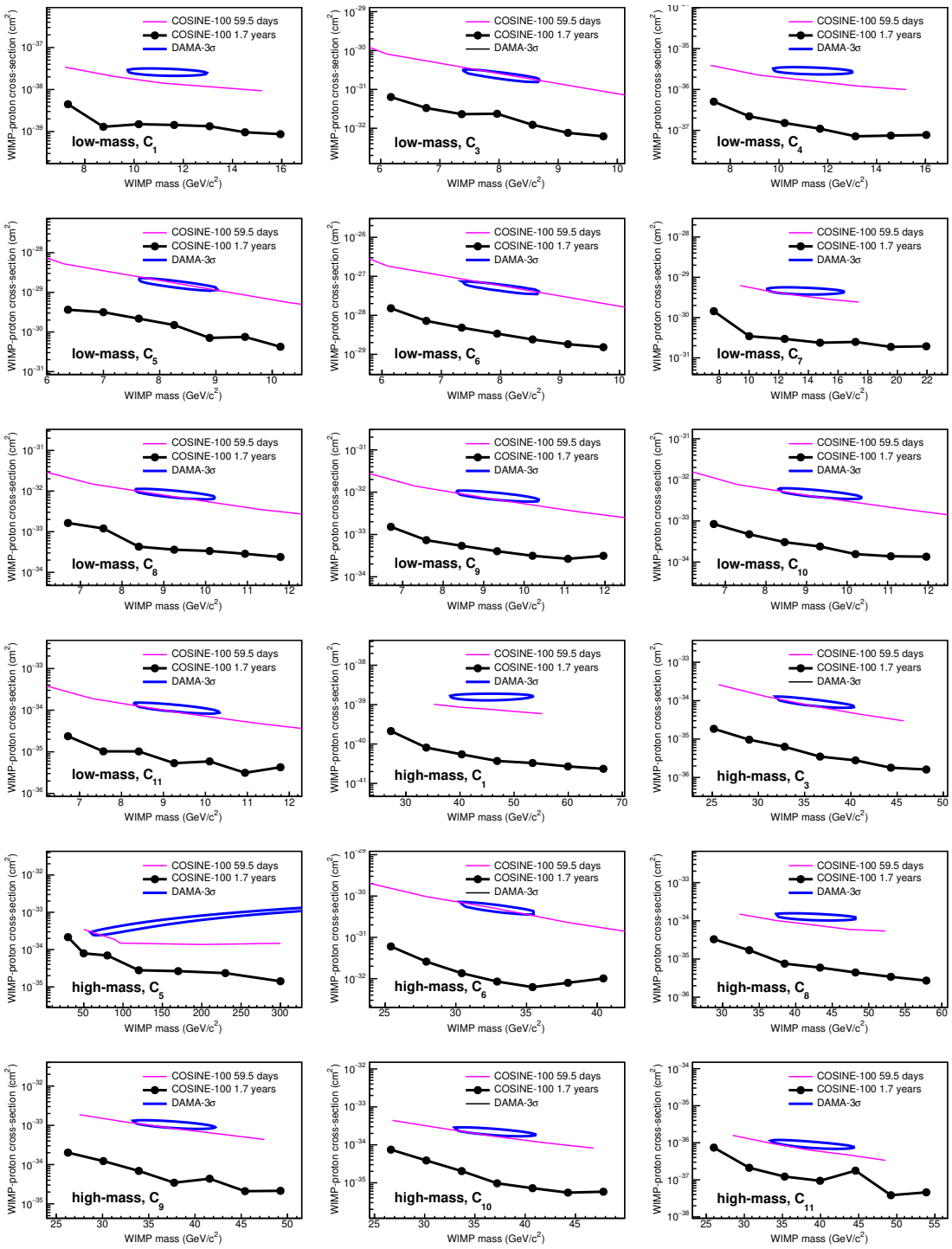

FIG. 4. **Exclusion limits on the WIMP-proton cross section for the effective field theory operators.** DAMA/LIBRA 3σ allowed regions (blue contours) and COSINE-100 90% confidence level exclusion limits of previous analysis (pink solid lines) and this work (black dots and lines) on the WIMP-proton cross sections for the effective field theory operators using same DAMA QF values are presented. For each operator, f_n/f_p is fixed to the corresponding best fit value of the DAMA/LIBRA data.

METHODS

event selection

An event satisfying the trigger condition of coincident photoelectrons in both of the crystal's readout PMTs within 200 ns is acquired with 500 MHz flash analog-to-digital converters and is recorded as 8 μs long waveforms starting 2.4 μs before occurrence of the trigger[18]. In the offline analysis, muon-induced events are rejected when the crystal hit event comes within 30 ms after a muon candidate event in the muon detector[17,31] and the crystal hit events to be less than 30 ms. Additionally, we require that leading edges of the trigger pulses start later than 2.0 μs after the start of the recording, that waveforms from the crystal contain more than two sub-pulses, and that the integral waveform area below the baseline does not exceed a limit. These criteria reject muon-induced phosphor events and electronic interference events. A multiple-hit event has accompanying crystal signals with more than four photoelectrons in an 8 μs time window or has a liquid scintillator signal above an 80-keV threshold within 4 μs[16]. A single-hit event is classified as one where the other detectors do not meet these criteria.

During the 1.7 years data-taking period, no significant environmental abnormality or unstable detector performance was observed. The high light yield of the six crystals, approximately 15 photoelectrons/keV, allowed an analysis threshold of 2 keV in the previous analysis. However, the other two crystals had lower light yields and required higher analysis thresholds of 4 keV and 8 keV respectively[4,8]. Since their direct impact on the WIMP search is not substantial, we do not include single-hit events from these two crystals in the WIMP search analysis, although they were used in the identification of multiple hits.

In the low-energy signal region below 10 keV, PMT-induced noise events predominantly contribute to the single-hit physics data in two different ways. The first class has a fast decay time of less than 50 ns compared with typical NaI(Tl) scintillation of about 250 ns. The second class, that occurs less often than the first, has different characteristics of slow rise and decay time, as characterized in Refs.[8,12]. Noise events of the second class are intermittently produced by certain PMTs. We have developed monitoring tools for data quality verification, including monitoring event rates of the second class of noise. If a crystal had an increased rate due to the second class of noise, the relevant period of data was

removed. One crystal detector had this class of noise for the whole period, but for the other five detectors more than 95 % of the recorded data could be used without the second-class noise-induced events.

A boosted decision tree (BDT) was developed to separate scintillation signals from the first class of noise. The fast PMT-induced events with energies greater than 2 keV were efficiently removed by the BDT, which is based on multiple parameters[8,12]: the balance of the deposited charge from two PMTs, the ratio of the leading-edge (0–50 ns) to trailing-edge (100 ns–600 ns) charge, and the amplitude weighted average time of the signal. However, using this BDT the scintillation events with energies below 2 keV were contaminated by an exponential increase in noise events.

We developed new parameters to characterize the PMT-induced noise events for efficient selection of the scintillation events below 2 keV. Two likelihood parameters for an event are constructed by templates derived from data samples enriched alternatively in scintillation-signal events and noise-signal events. A ^{60}Co source that produces low energy electron signals through Compton scattering is used to generate the signal enriched sample. Fast decay events in the single-hit data sample are used as the noise enriched sample.

The likelihood parameter of the event is calculated as,

$$\ln \mathcal{L} = \sum_i \left[T_i - W_i + W_i \ln \frac{W_i}{T_i} \right], \tag{1}$$

where T_i and W_i are the height of the i^{th} time bin in the reference template and event, respectively. Likelihood parameters for the scintillation signal events ($\ln \mathcal{L}_s$) and the PMT-induced noise events ($\ln \mathcal{L}_n$) are evaluated for each event. With these, we define a likelihood score as,

$$p_l = \frac{\ln \mathcal{L}_n - \ln \mathcal{L}_s}{\ln \mathcal{L}_n + \ln \mathcal{L}_s}, \tag{2}$$

where large p_l for an event implies that the event is more closely matched to the scintillation signal than the PMT-induced noise events. The updated BDT is trained with the likelihood score. This provided good discrimination against PMT-induced noise events and enabled us to lower the threshold to 1 keV[15]. A BDT score, a single discriminating parameter created by combining the various selections for input parameters according to their corresponding

importance, for the single-hit physics data near the energy threshold (1–1.25 keV) is presented in Extended Data Fig. 1. With the established selection criteria, we reduced the PMT-induced noise contamination level to less than 0.5 %.

Event selection efficiencies for the electron recoil events were evaluated with the ^{60}Co calibration data. The efficiency is calculated by integrating the model distribution of the scintillation signals and the PMT-induced noise events shown in Extended Data Fig. 1. A specialized apparatus with a monoenergetic 2.42 MeV neutron beam was used to measure the selection efficiencies of the nuclear recoil events[21]. This measurement was performed with a small-size test crystal that was cut from the same ingot of a crystal used for the COSINE-100 experiment. The efficiencies determined for the electron recoil events and the nuclear recoil events are consistent within the 5% level as shown in Extended Data Fig. 2. Systematic uncertainties in the efficiency measurements account for deviations from different measurements, as well as from the ^{60}Co calibration data and the single-hit physics data.

background modeling

Events are classified according to their energy: 1–70 keV are low energy and 70–3000 keV are high energy. The single-hit and multiple-hit data are separated in the background modeling of the NaI(Tl) crystals. To understand background spectra, Geant4-based simulation events are generated and recorded in a format that matches that of the COSINE-100 data acquisition system. The energy resolutions and selection efficiencies for each crystal are applied. The fraction of each background component is determined from a simultaneous fit to the four measured distributions. For the single-hit events, only 6–3000 keV events are used to avoid a bias of the WIMP signal in the region of interest (ROI). Details of the background modeling for the dataset are described elsewhere[19].

The background components are divided into four categories: internal contamination, surface contamination, external sources and cosmogenic activation. The ^{238}U, ^{232}Th, ^{40}K, and ^{210}Pb contaminations in the crystal constitute the internal background. The ^{210}Pb contaminations on the crystal surface and adjacent materials are the surface component. Backgrounds from ^{238}U, ^{232}Th and ^{40}K in the PMTs, liquid scintillator, and the shield materials constitute external sources. In order to estimate contributions from cosmogenic activation, we use a time-dependent analysis that takes into account the cosmic-ray exposure

time on the ground and the cooling time in the underground laboratory of each individual crystal[30].

The most dominant background components in the ROI are generated by internal radionuclide contamination and by cosmogenic activation. This includes ^{210}Pb and ^{40}K internal contaminants, and surface contamination by ^{210}Pb. The contribution in the ROI by cosmogenic activation is mostly due to ^{3}H with some additional contributions from ^{113}Sn and ^{109}Cd. Background modeling was performed independently for each individual crystal, and Extended Data Fig. 3 shows the accumulated result of the model fit to data and the systematic uncertainties.

systematic uncertainties

In addition to the statistical uncertainties in the background and signal models, various sources of systematic uncertainties are taken into account. Errors in the selection efficiency, the energy resolution, the energy scale, and background modeling technique translate into uncertainties in the shapes of the signal and background probability density functions, as well as to rate changes. These quantities are allowed to vary within their uncertainties as nuisance parameters in the likelihood fit.

The most influential systematic uncertainty is the error associated with the efficiencies shown as the shaded region in Extended Data Fig. 1. This is because the efficiency systematic uncertainty that maximally covers the statistical uncertainties in the ROI mimics the shape expected for a WIMP signal. In the background model fit, background activities are constrained by Gaussian constraint terms added to the likelihood function as determined by measured activities and their uncertainties. And the systematic uncertainties associated with the background modeling include the uncertainties of the activities estimated by the background model fit. In addition, different locations of external radioactive contaminations are taken into account by generating external contributions at different positions. Background contributions from ^{210}Pb contamination on the surface of the NaI(Tl) crystals were studied with a small NaI(Tl) crystal exposed to ^{222}Rn from a ^{226}Ra source[24]. Depth profiles from two exponential components were modeled to fit the ^{222}Rn contaminated crystal and matched to the test-setup data[19]. Uncertainties in the measured depth profiles are propagated into systematic uncertainties.

The energy calibration is performed by tracking the positions of internal β and γ peaks from radioactive contaminations in the crystals, as well as with external γ sources[19]. The nonlinear detector response of the NaI(Tl) crystals[23] in the low energy region is modeled with an empirical function across all crystals[19]. Subtle differences for each crystal from the general nonlinearity model of the NaI(Tl) crystals are evaluated to consider the systematic uncertainty on the energy scale. The energy resolution for each crystal is evaluated during the calibration process. In particular, tagged 0.8 keV (^{22}Na) and 3.2 keV (^{40}K) X-ray lines in the multiple-hit data are used to determine the energy resolution for low-energy events. Statistical uncertainties associated with the number of tagged events are regarded as the resolution systematic. Extended Data Fig. 3 shows a comparison of the background model to the data together with $\pm1\sigma$ and $\pm2\sigma$ bands of the systematic uncertainties that are evaluated from the quadrature sum of each systematic component.

expected WIMP signal

The differential nuclear recoil rate[32] per unit target mass for elastic scattering between WIMPs of mass m_χ and target nuclei of mass M is,

$$\frac{dR}{dE_{\rm nr}} = \frac{2\rho_\chi}{m_\chi} \int d^3v \; v \; f(\mathbf{v},t) \; \frac{d\sigma}{dq^2}(q^2,v), \tag{3}$$

where ρ_χ is the local dark matter density, $f(\mathbf{v},t)$ is the time-dependent WIMP velocity distribution and $\frac{d\sigma}{dq^2}(q^2,v)$ is the differential cross section depending on the velocity with the momentum exchange $q^2 = 2ME_{\rm nr}$.

For the WIMP velocity distribution, we assume a Maxwellian distribution[32],

$$f(\mathbf{v},t) = \frac{1}{N_{\rm esc}} \; e^{-(\mathbf{v}+\mathbf{v}_{\rm E})^2/2\sigma_v^2}, \tag{4}$$

where $N_{\rm esc}$ is a normalization constant, v_E is the Earth velocity relative to the WIMP dark matter and σ_v is the velocity dispersion. The standard halo parameterization is used with the local dark matter density $\rho_\chi = 0.3$ GeV/cm^3, $v_E = 232$ km/s, $\sqrt{2}\sigma_v = 220$ km/s and the galactic escape velocity $v_{\rm esc} = 544$ km/s.

The effective field theory operators and nuclear form factors described in Refs.[33–36] are used to model the nuclear responses in the differential cross section. The generalized spin-

independent response[35] is used for both the isospin-conserving and the isospin-violating spin-independent (SI) interactions. For isospin-violating SI interactions, the WIMP-nucleon coupling coefficient ratio, f_n/f_p is fixed to the best fit values for the DAMA/LIBRA data[14]. These nuclear responses, including form factors, are implemented using the publicly available DMDD package[37] to evaluate the differential nuclear recoil rate $dR/dE_{\rm nr}$ (raw signal spectra). We subsequently apply the quenching factors, energy resolution, and selection efficiency to obtain the expected nuclear recoil rate in electron-equivalent energy for the detector, $dR/dE_{\rm ee}$. Extended Data Fig. 4 shows $dR/dE_{\rm nr}$ (a) and $dR/dE_{\rm ee}$ (b) spectra for three different WIMP models assuming WIMP-proton cross section equal to 1 pb.

In addition, we generate the WIMP signals in the context of the non-relativistic effective theory of WIMP-nucleus scattering that has been tested using previous data without full coverage of the DAMA/LIBRA 3σ allowed regions[12]. For simplicity we assume that one of the effective operators allowed by Galilean invariance dominates in the effective Hamiltonian of a spin-half dark matter particle at a time. We use the best-fit neutron-over-proton coupling ratio of the DAMA/LIBRA-phase2 data assuming the DAMA QF, which is obtained in Ref.[38], for each operator. The DMDD package[37] is also used to generate signal spectra by the effective operators. A few operators are not evaluated because the DMDD package does not include form factors for these operators. Here, we assume the same DAMA QFs for the COSINE-100 data for a simple comparison.

Bayesian approach

A Bayesian approach is adopted to extract the WIMP signal from the COSINE-100 data. For each WIMP interaction model, a posterior probability density in terms of the WIMP-proton cross section $\sigma_{\rm WIMP}$ is obtained from the Bayes' theorem[39] using a marginalization of the likelihood function that includes the prior[26],

$$P(\sigma_{\rm WIMP}|\mathbf{M}) = N \cdot \int \mathcal{L}(\mathbf{M}|\sigma_{\rm WIMP},\ \boldsymbol{\alpha}) \cdot \pi(\boldsymbol{\alpha})\ d\boldsymbol{\alpha}, \tag{5}$$

where $P(\sigma|\mathbf{M})$ is a posterior probability density function (PDF) and $\mathcal{L}(\mathbf{M}|\sigma,\boldsymbol{\alpha})$ is the likelihood function. The prior $\pi(\boldsymbol{\alpha})$ constrains the systematic uncertainties and the normalization constant N makes the integration of the posterior PDF to be unity. The $\mathbf{M}$ represents the measured data and $\boldsymbol{\alpha}$ represents the nuisance parameters.

Because the measurements are independent and follow Poisson probabilities, the likelihood function is built by a product of Poisson probabilities,

$$\mathcal{L}(\mathbf{M}|\sigma_{\rm WIMP},\ \boldsymbol{\alpha}) = \prod_{i}^{N_{\rm crystal}} \prod_{j}^{N_{\rm bin}} \frac{[B_{ij}(\boldsymbol{\alpha}) + S_{ij}(\sigma_{\rm WIMP},\ \boldsymbol{\alpha})]^{M_{ij}}}{M_{ij}!} e^{-[B_{ij}(\boldsymbol{\alpha}) + S_{ij}(\sigma_{\rm WIMP},\ \boldsymbol{\alpha})]}, \tag{6}$$

where i and j denote the crystal number and the energy bin, respectively, and M_{ij} is the observed event rate for $i^{\rm th}$ crystal in $j^{\rm th}$ energy bin. The number of background events $B_{ij}(\boldsymbol{\alpha})$ and signal events $S_{ij}(\sigma, \boldsymbol{\alpha})$ are generated from the simulated experiments through the background modeling and the WIMP signal discussed above, with effects by systematic uncertainties. The systematic uncertainty affecting the background model is included as a function of the nuisance parameter $\boldsymbol{\alpha}$, as

$$B_{ij}(\boldsymbol{\alpha}) = \prod_{k}^{N_{\rm syst}} (1 + \alpha_{ik}\epsilon_{ijk}) \cdot B_{ij}^{\rm MC}, \tag{7}$$

where the expected background components in $j^{\rm th}$ energy bin of crystal i including the systematic uncertainty, $B_{ij}(\boldsymbol{\alpha})$, is expressed with α_{ik}, $k^{\rm th}$ nuisance parameter, ϵ_{ijk}, the relative error of the $k^{\rm th}$ systematic uncertainty, and $B_{ij}^{\rm MC}$, the number of background events obtained by modeling. Similar impact for the WIMP signal is considered through the following formula,

$$S_{ij}(\sigma_{\rm WIMP},\ \boldsymbol{\alpha}) = \prod_{k}^{N_{\rm syst}} (1 + \alpha_{ik}\epsilon_{ijk}) \cdot T_i \cdot M_i \cdot R_j(\sigma_{\rm WIMP}; m_\chi), \tag{8}$$

where M_i and T_i denote the mass and data exposure for i crystal, and R_j is the expected rate of WIMP-proton interaction through an integration of $dR/dE_{\rm ee}$ in the $j^{\rm th}$ energy bin.

The rate of each background or signal component are affected by all nuisance parameters, and some of those parameters, such as parameters for selection efficiency, energy scale, and energy resolution, can affect the spectral shape. Each $k^{\rm th}$ nuisance parameter is constrained with evaluated uncertainty assuming Gaussian distribution,

$$\pi(\boldsymbol{\alpha}) = \prod_{i}^{N_{\rm crystal}} \prod_{k}^{N_{\rm syst}} e^{-\alpha_{ik}^2}. \tag{9}$$

The Markov Chain Monte Carlo[40,41] via Metropolis-Hastings algorithm[42,43] is used for the

multivariable integration in posterior PDF. We developed our own Bayesian tool for this process. A comparison with a publicly available Bayesian analysis toolkit[44] was done for the initial 59.5 days COSINE-100 data and both tools showed consistent results.

To avoid biasing the WIMP search, the fitter was tested with simulated event samples. Each experimental data is prepared by Poisson random extraction from the modeled background spectrum[19], assuming a background only hypothesis. Marginalization to obtain the posterior PDF for each simulation sample is performed to set the 90% confidence level exclusion limit as shown in Extended Data Fig. 5. The 1000 simulated experiments result in 68% and 95% bands of the expected limit as presented in Figs. 2 and 3.

The data fits are done in the same way as the simulated data. Extended Data Fig. 5 shows the posterior PDFs and their cumulative distribution functions (CDFs) of data for two different WIMP models. The CDF provides the 90% confidence level exclusion limit for each fit.

REFERENCES

[31]H. Prihtiadi et al., (COSINE-100 Collaboration), Measurement of the cosmic muon annual and diurnal flux variation with the COSINE-100 detector, JCAP **02**, 013 (2021).

[32]J. Lewin and P. Smith, Review of mathematics, numerical factors, and corrections for dark matter experiments based on elastic nuclear recoil, Astropart. Phys. **6**, 87 (1996).

[33]V. Gluscevic, M. I. Gresham, S. D. McDermott, A. H. G. Peter, and K. M. Zurek, Identifying the Theory of Dark Matter with Direct Detection, JCAP **1512**, 057 (2015).

[34]N. Anand, A. L. Fitzpatrick, and W. C. Haxton, Weakly interacting massive particle-nucleus elastic scattering response, Phys. Rev. C **89**, 065501 (2014).

[35]A. L. Fitzpatrick, W. Haxton, E. Katz, N. Lubbers, and Y. Xu, The Effective Field Theory of Dark Matter Direct Detection, JCAP **1302**, 004 (2013).

[36]M. I. Gresham and K. M. Zurek, Effect of nuclear response functions in dark matter direct detection, Phys. Rev. D **89**, 123521 (2014).

[37]V. Gluscevic and S. D. McDermott, dmdd: Dark matter direct detection, Astrophysics Source Code Library [ascl:1506.002], 2015.

[38]S. Kang, S. Scopel, G. Tomar, and J.-H. Yoon, DAMA/LIBRA-phase2 in WIMP effective models, JCAP **1807**, 016 (2018).

[39]J. Joyce, Bayes Theorem, in *The Stanford Encyclopedia of Philosophy* (E. N. Zalta, ed.). Metaphysics Research Lab, Stanford University, spring 2019 ed., 2019.

[40]W. Gilks, S. Richardson, and D. Spiegelhalter, *Markov Chain Monte Carlo in Practice*. Boca Raton: Chapman & hall/CRC, 2006.

[41]D. Gamerman and H. F. Lopes, *Markov Chain Monte Carlo*. Boca Raton: Chapman & hall/CRC, 2006.

[42]N. Metropolis, A. W. Rosenbluth, M. N. Rosenbluth, and A. H. Teller, Equation of State Calculations by Fast Computing Machines, J. Chem. Phys. **21**, 1087 (1953).

[43]W. K. Hastings, Monte carlo sampling methods using markov chains and their applications, Biometrika **57**, 97–109 (1970).

[44]A. Caldwell, D. Kollar, and K. Kroninger, BAT: The Bayesian Analysis Toolkit, Comput. Phys. Commun. **180**, 2197 (2009).

Code availability The analysis codes that support the findings of the study are available from the corresponding authors upon reasonable request.

Data availability The data that support the findings of this study are available from the corresponding authors upon reasonable request.

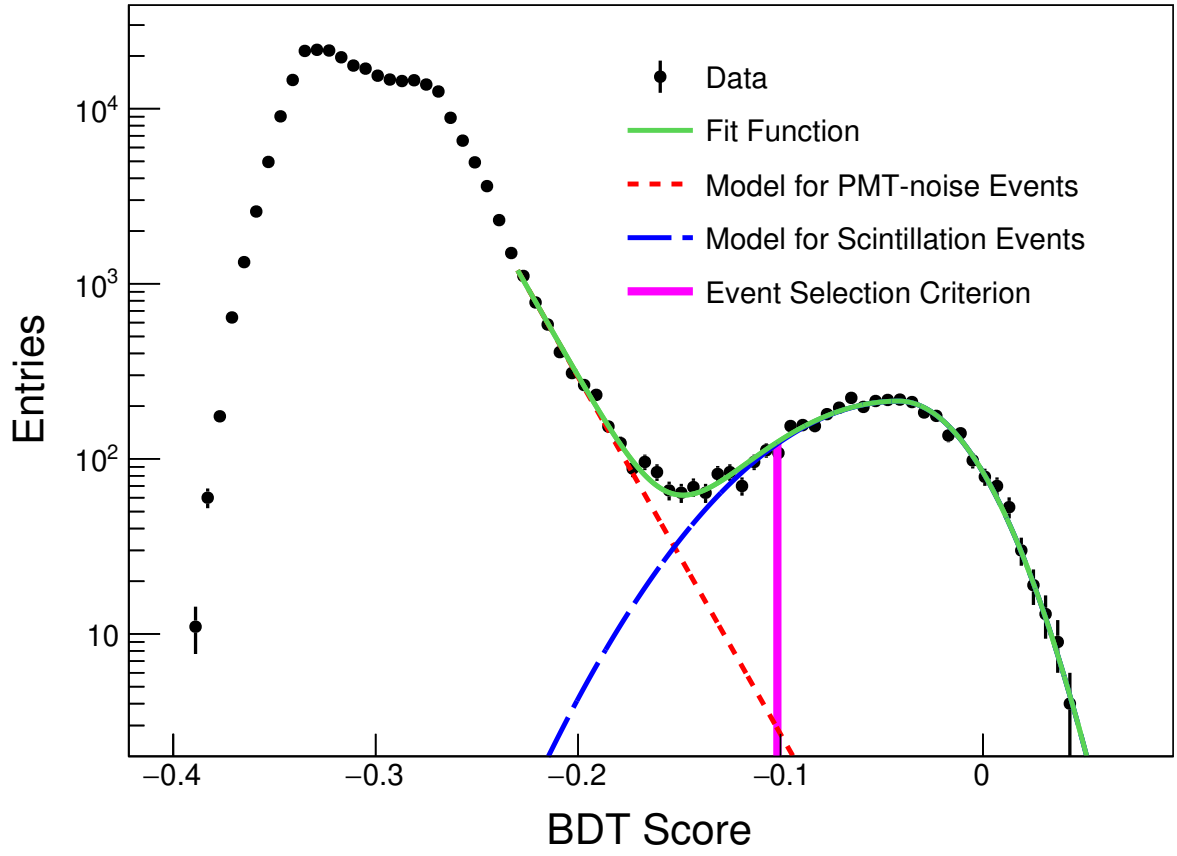

Extended Data Fig. 1. **BDT-score distribution of events at the 1–1.25 keV.** The BDT distribution of the single-hit physics data is fitted by the green function that consists of an asymmetric Gaussian distribution for the scintillation events (dashed blue) and an exponential function for the PMT-noise events (dotted red). The thick magenta line shows a BDT criterion for the event selection.

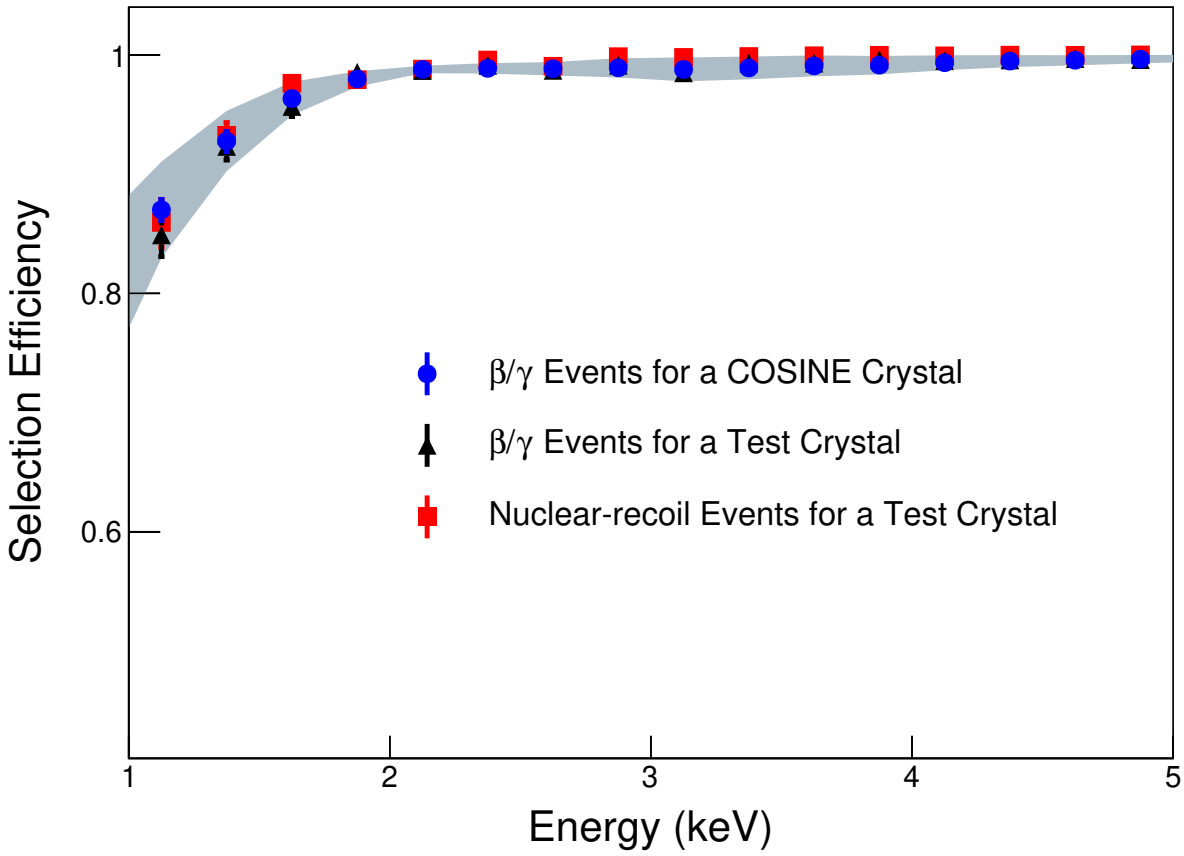

Extended Data Fig. 2. **Efficiencies of β/γ and nuclear-recoil events.** Blue dots show the efficiencies of β/γ events for a COSINE-100 crystal. Black and red dots are efficiencies of β/γ and nuclear-recoil events, respectively, for a small-size test crystal. This test crystal was cut from the same ingot of the COSINE-100 crystal and used for the neutron beam measurement. All measurements are consistent within the systematic uncertainty of the efficiency shown in grey band.

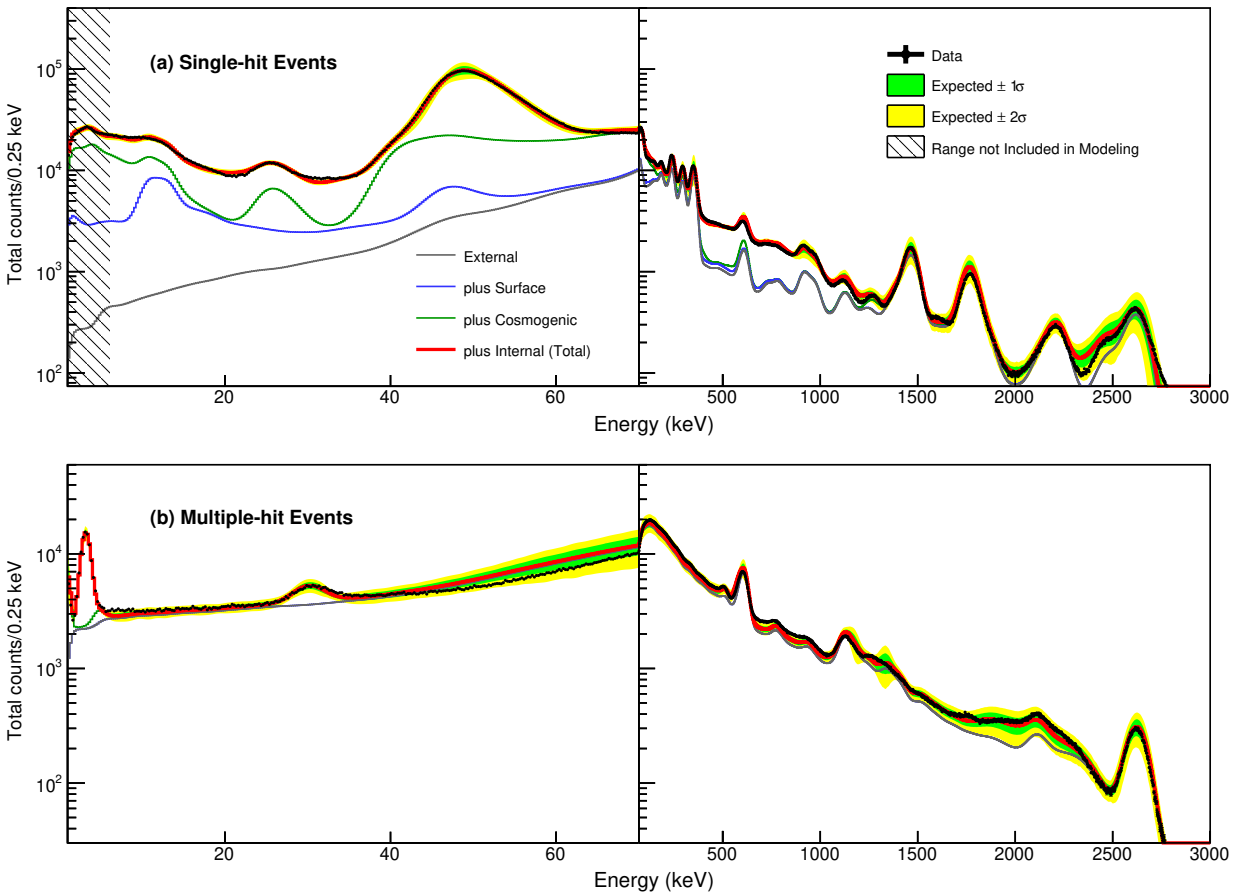

Extended Data Fig. 3. **Energy spectra of single-hit and multiple-hit events.** Presented here are summed energy spectra for the five crystals (black dots) and their background modeling (red solid line) with the 68% and 95% confidence intervals. The expected contributions to the background from internal radionuclide contaminations, the surface of the crystals and nearby materials, cosmogenic activation, and external backgrounds are indicated. Where the single-hit 1–6 keV is masked because these events are not used for the background modeling.

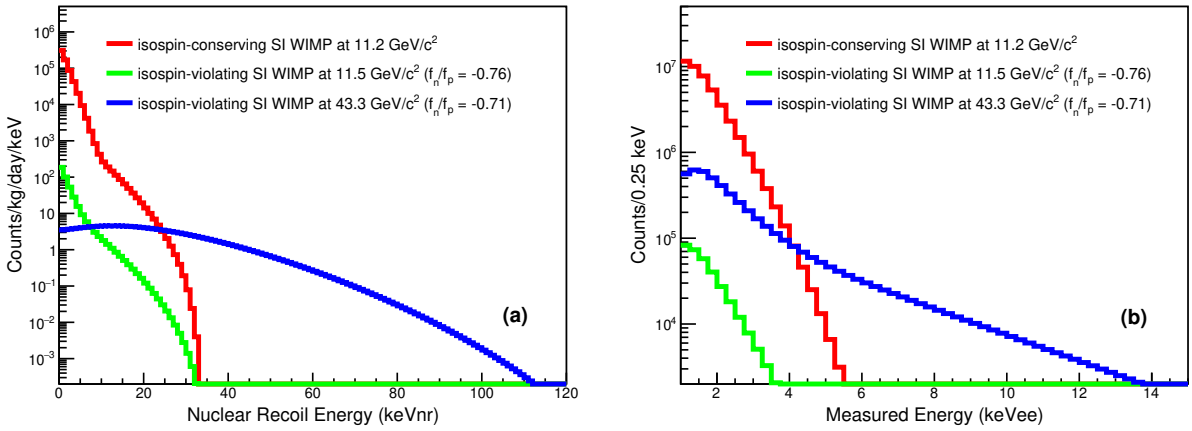

Extended Data Fig. 4. **Energy spectra of the WIMP signal.** (a) Raw energy spectra for three different WIMP models with WIMP-proton cross section of 1 pb. (b) The expected energy spectra with WIMP-proton cross section of 1 pb for the three WIMP models when taking account of the quenching factors, detector resolutions, and selection efficiencies assuming 1.7 years COSINE-100 data.

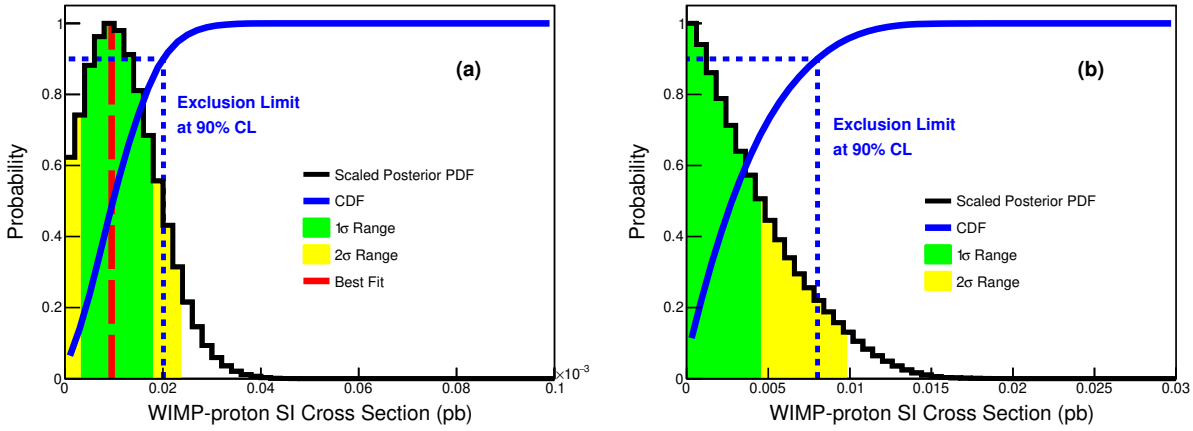

Extended Data Fig. 5. **Posterior probability density functions.** Two examples of the posterior PDFs and their CDFs for the 1.7 years COSINE-100 data for different WIMP models. (a) is the canonical model for a WIMP mass of 20.4 GeV/c^2 and (b) is the isospin-violating case with WIMP mass 11.5 GeV/c^2 and $f_n/f_p = -0.76$. The posterior PDFs are scaled for the maximum to be unity. The exclusion limit at 90% confidence level is obtained from CDF matched with 0.9. Green and yellow areas represent the 68% and 95% of confidence intervals, respectively. In the case of (a), the best fit value (red-dashed line) presents slightly positive result of WIMP-proton cross section 9.5×10^{-5} pb, but within 95% region. We, therefore, set the 90% confidence level upper limit.

Figures

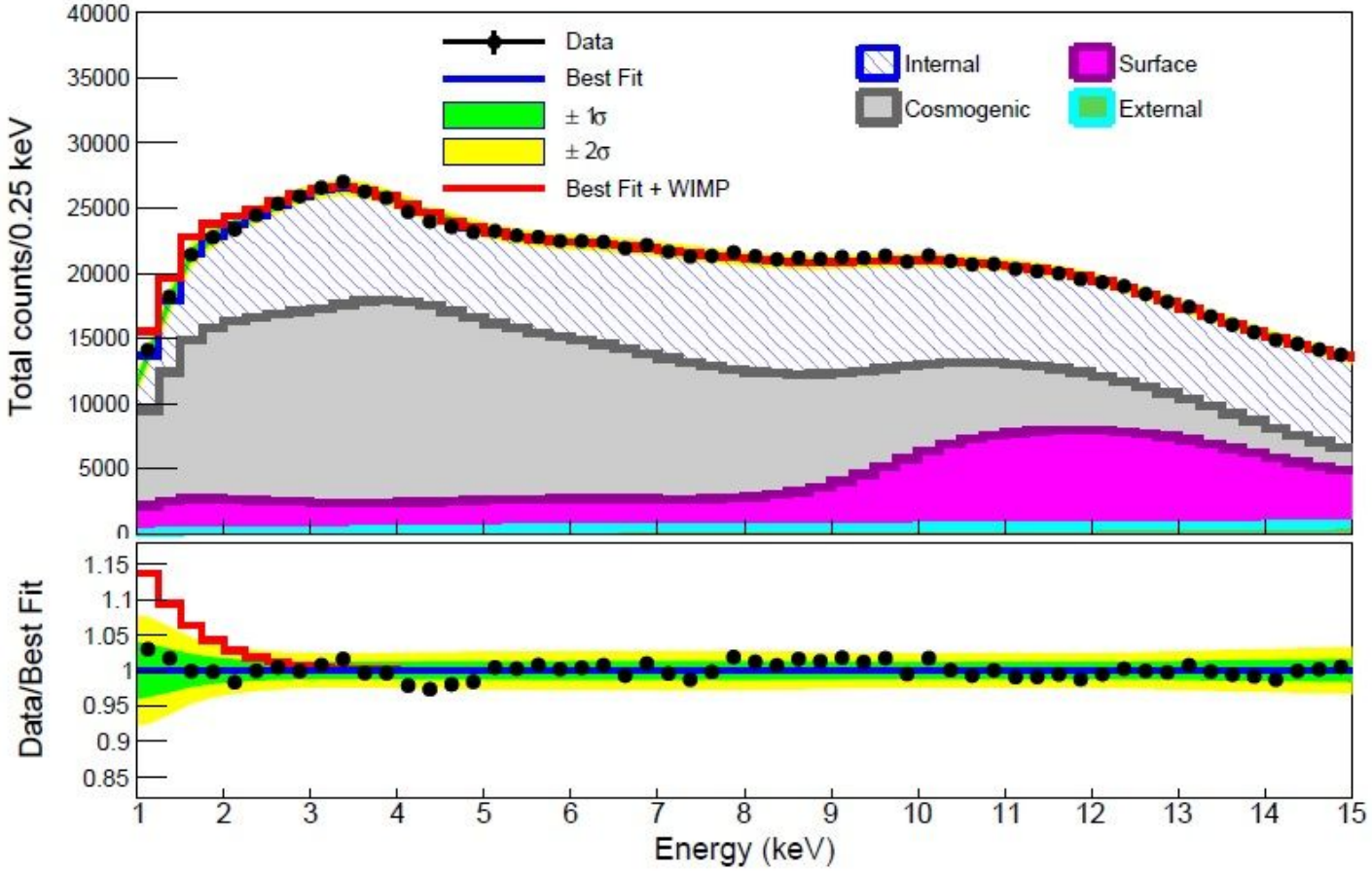

Figure 1

Example t results for a 11.5 GeV/c2 WIMP mass in the case of fn=fp =-0:76 (see Manuscript file for full figure caption)

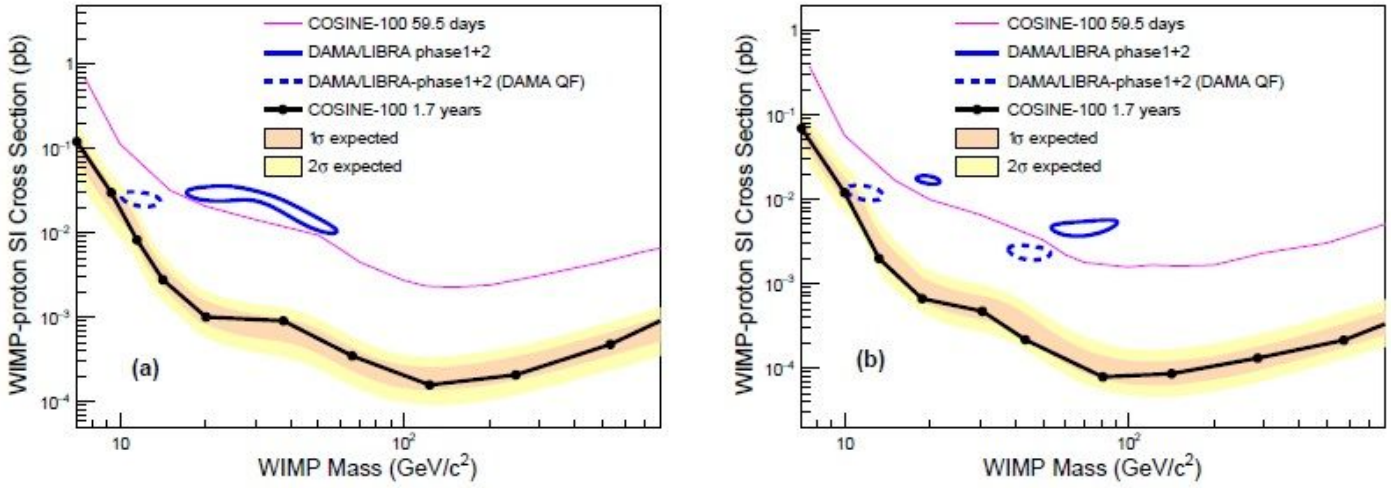

Figure 2

Exclusion limits on the WIMP-proton spin-independent cross section for the isospin-violating interaction. (see Manuscript file for full figure caption)

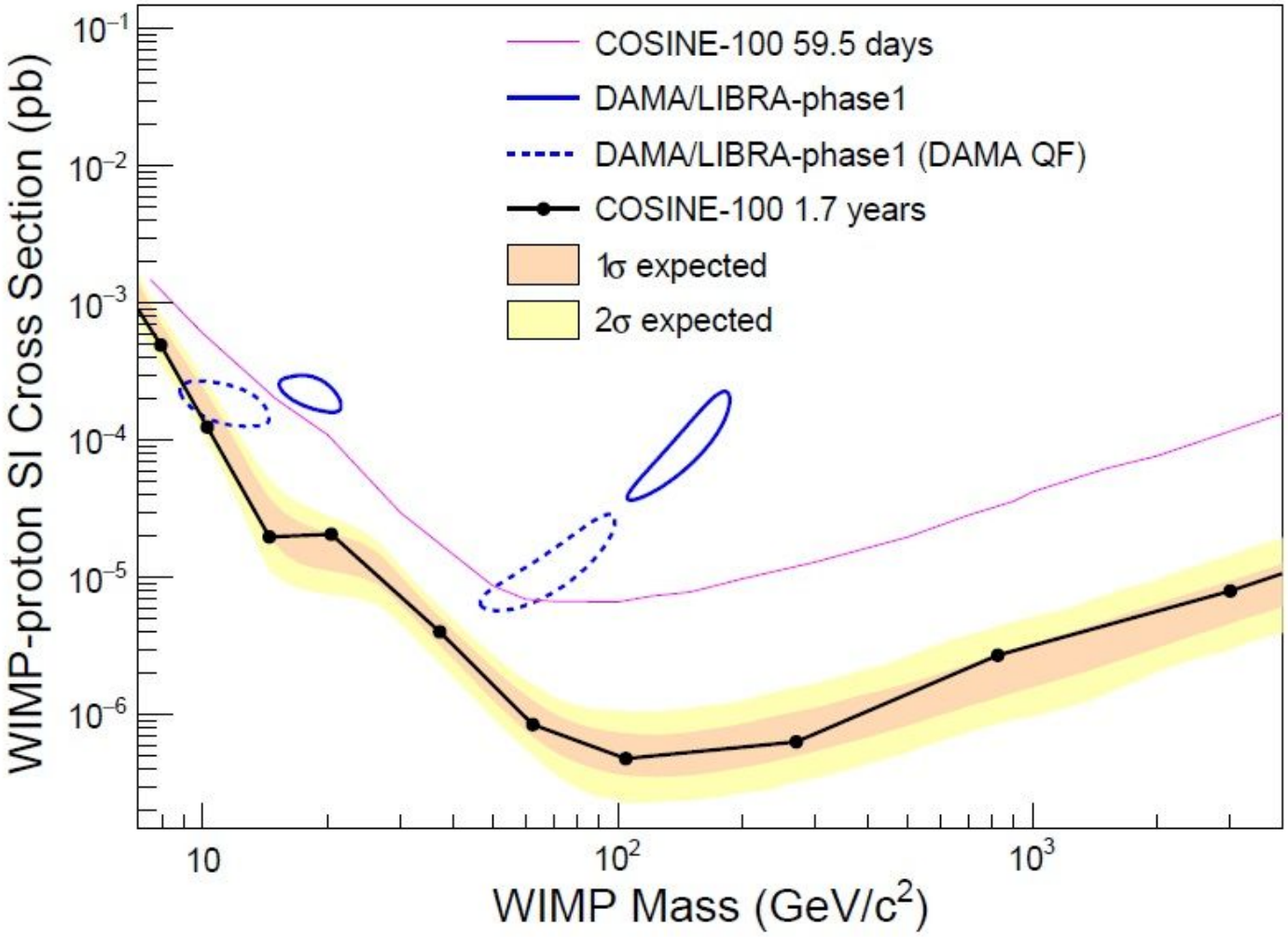

Figure 3

Exclusion limits on the WIMP-nucleon spin-independent cross section of the isospin-conserving interaction. (see Manuscript file for full figure caption)

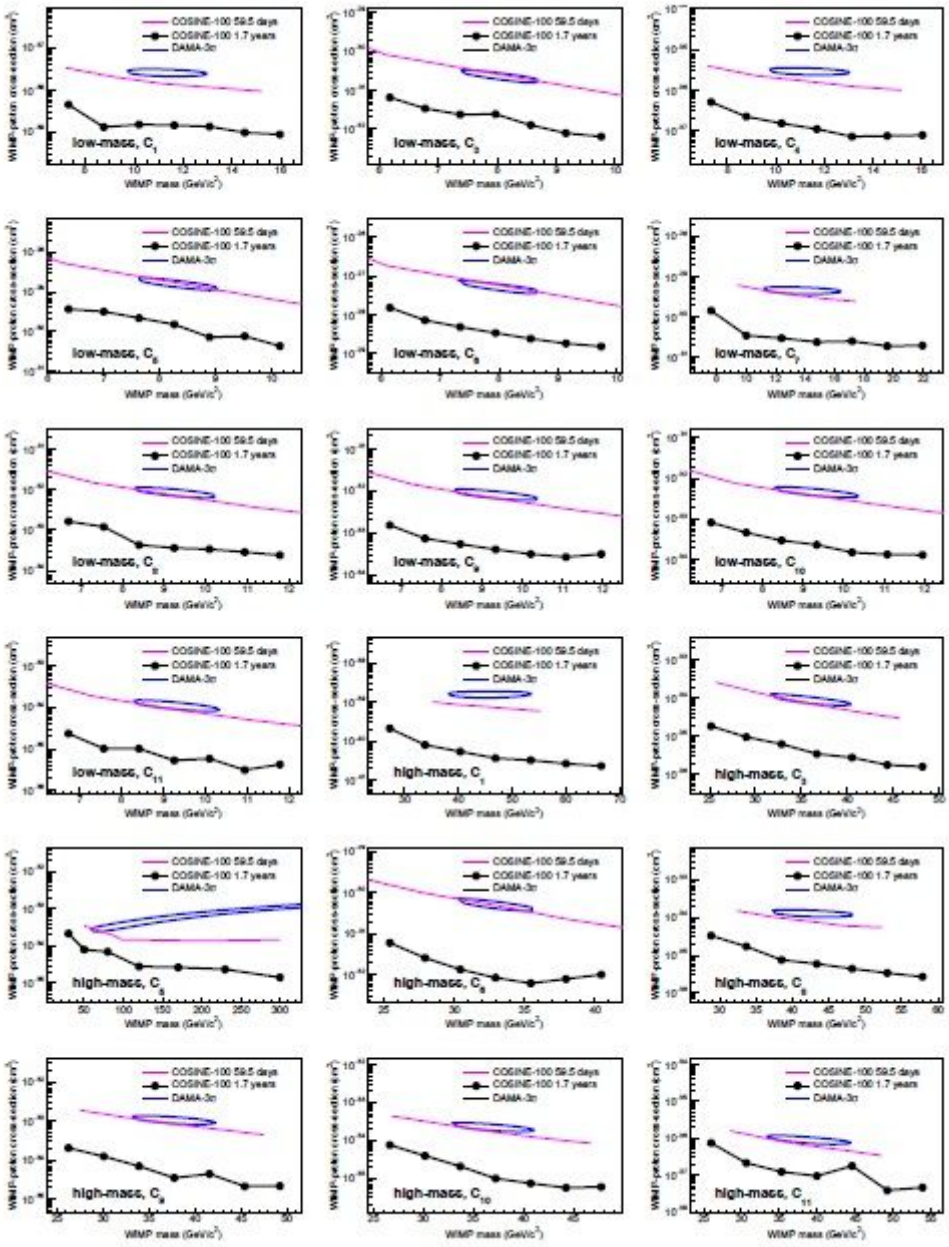

Figure 4

Exclusion limits on the WIMP-proton cross section for the effective field theory operators. (see Manuscript file for full figure caption)